Ligand Nanocluster Array Enables Artificial-Intelligence-Based Detection of Hidden Features in T-Cell Architecture

Aya Nassereddine, Ahmed Abdelrahman, Emmanuelle Benard, F. Bedu, Igor Ozerov, Laurent Limozin, Kheya Sengupta

Ligand nano-cluster array enables AI based detection of hidden features in T cell architecture

Aya Nassereddine,[†,‡] Ahmed Abdelrahman,[†,‡] Emmanuelle Benard,[†] Frederic Bedu,[†] Igor Ozerov,[†] Laurent Limozin,[*,‡] and Kheya Sengupta[*,†]

[†]*Aix Marseille Univ, CNRS, CINAM, Marseille, 13009 France.*

[‡]*Aix Marseille Univ, CNRS, INSERM, LAI, Marseille, 13009 France.*

E-mail: laurent.limozin@inserm.fr; sengupta@cinam.univ-mrs.fr

Phone: +33 (0)4 91 17 28 00 . Fax: +33 (0)4 91 41 89 16

Abstract

Protein-patterning has emerged as a powerful means to interrogate adhering cells. Yet, the tools to apply a sub-micron periodic stimulus and the analysis of the response are still being standardized. We propose a technique combining electron-beam lithography and surface functionalization to fabricate nano-patterns compatible with advanced imaging. The repetitive pattern enables a deep-learning algorithm to reveal that T cells organize their membrane and actin network differently depending on whether the ligands are clustered or homogeneously distributed - an effect invisible to the unassisted human eye even after extensive image analysis. This fabrication and analysis tool-box should be useful, both together and separately, for exploring general correlation between a spatially-structured sub-cellular stimulation and a subtle cellular response.

Keywords

Nano-patterning, lithography, surface functionalisation, deep learning, T cell

Introduction

Nanopatterning of biomolecules on inorganic surfaces is currently an important tool for bioengineering and cutting-edge cell biology studies. Experiments on cellular interactions with such patterned surfaces provide insights into the mechanisms of cell adhesion, activation and signalling. This knowledge in turn is used to optimize the performance of, for example, artificial soft tissue grafts and prostheses.[1–4] In the context of cell biology and bioengineering, arrays of solid-supported submicro/nano scaled protein dots are currently used to influence cell architecture and to decipher cell function. There is therefore tremendous interest in the cell biology, as well as specialized fields like immunology and neuroscience, biophysics and bioengineering/biomedical community to study the interaction of cells with patterned substrates.[5–7] However, there are only few techniques to make such substrates, that must fulfil a long list of requirements ranging from non-toxicity, to large surface coverage, to being fully compatible with state-of-art optical imaging.[8,9] Self-assembly, including by DNA-origami[10–13] and serial-writing are two popular tools to create nano-bio-patterns. The advantage of serial-writing, for example using an electron-beam is that the control over the pattern geometry is total .[14,15] The advantage conferred by regular geometry is exploitable in image analysis, including, by deep learning, a strategy that has become important in recent times.[16–19] An additional advantage is conferred when the pattern is metal-free,[9,20] since specialized techniques like TIRF and super-resolution imaging become impossible in presence of high density metal features due to their interaction with light, including the risk of generating a plasmonic response.

T-cells are particularly intriguing candidates for testing a possible correlation between the distribution of a clustered stimulus, and the response of the cell. Sub-micron sized clus-

ters of the T cell receptor (TCR), called TCR μ-clusters, play a crucial role in amplification of feeble signals, provided by rare agonist peptides, to cell scale and eventually organism scale response.[21–23] Actin is a key player in this amplification but, though it is known that TCR molecules interact with the actin cytoskeleton, the structural link between the two is yet to be elucidated. Specifically, whether or not the geometry of the TCR μ-clusters is reflected in actin organization[24–27] is not known.

Early studies established that micron-scale patterning of ligands can drastically reorganise surface receptor distribution in T cells and completely disrupt the formation of late-time ordered synapses,[28,29] an effect also seen when barriers are put to prevent ligand-receptor pairs from reorganizing,[30,31] which however may not reorganize the actin.[31] At early times during T cell spreading, TCR microclusters get coupled to the actin retrograde flow[32] and are implicated in force transduction.[33,34] Modification of T-cell membrane protein distribution,[35] and colocalisation of TCR-microclusters with patterned ligands of TCR,[36,37] was previously demonstrated. Ligand presentation as nano-scale pattern also impacts T cell spreading and activation, however, the interpretation remains complex[38–40]

In order to explore the role of TCR μ-clusters in determining actin architecture, we exploit previous finding that clustering of TCR-ligands or antibodies against the TCR complex can induce clustering of TCRs themselves[8,36,37,41] to generate stable TCR μ-clusters arranged in an array. We leverage the ability of e-beam lithography to create flawless arrays of a repeated motif, to decipher the impact of presenting TCR-ligand-clustering on actin organization. We present T-cells with a regular array of metal-free nano-dots of functionalized proteins, with size ranging from 250 nm to 700 nm diameter, and displaying an antibody against the CD3 domain of the T cell receptor. This new protocol combines e-beam lithography with stepwise surface functionalisation.[9,42,43] The actin in T cells is imaged in total internal reflection fluorescence (TIRF) microscopy and the membrane in reflection interference contrast microscopy (RICM). The images are analysed using a novel application of deep learning where

the ability of a binary classifier to correctly classify a presented local cell-feature, influenced or not by the ligand micro-cluster, is taken as the indicator of dissimilarity between the two categories. We show that indeed the TCR clustering does impact the local actin organization and membrane topography, though the nature of the resulting effect could not be identified.

To fabricate the protein nano-dot array, we adapt a two stage strategy. In the first stage (SI fig. 1-4), carried out in a clean room, a glass cover-slide is cleaned and spin-coated with an e-beam lithography resist. An electron beam is used to write the desired pattern on the resist, followed by standard lithographic development to remove unexposed area to obtain a surface covered with pillars of cross-linked resist. Each slide has 6 square regions (500 μm X 500 μm), each patterned with dots arranged in a centred-hexagonal lattice with putative dot diameter and lattice spacing of 700 nm and 2 μm (called E700), 400 nm and 1 μm (E400), or 250 nm and 1 μm (E250) (Fig. 1 a). Aluminium metal is evaporated on the substrate and finally, the pillars of cross-linked resist are removed by chemical lift-off. At this point, the slide is covered with a layer of aluminium with holes exposing bare glass underneath.

The second stage, consisting of surface functionalization (Fig. 1 b and SI Fig. 7), is carried out in a standard wet-laboratory, following a protocol previously established in the context of patterns created from self-assembled colloidal beads.[9,42] Briefly, the steps consist of vapour deposition of an organo-silane (APTES) on to the exposed glass and deposition of a place-holder protein (biotin-BSA) from solution. This is followed by chemical removal of the aluminium layer, leaving behind islands of biotin-BSA on bare glass. The glass is then back-filled either with a co-polymer of poly(L-lysine) and poly(ethylene glycol) (PLL-PEG), or with a supported lipid bilayer (SLB, see SI for details). The biotin-BSA islands can then be functionalized with neutravidin and finally a biotinylated protein, here anti-CD3, which targets the TCR complex in T cells (Fig. 1 b).

In order to visualize the pattern, we used fluorescent neutravidin (NaV) which shows up as an array of dots within a sea of invisible PLL-PEG or SLB (Fig. 1 c and SI Fig. 3, While PLL-PEG or SLB can be equivalently used, the data presented herein are from PLL-PEG

back-filling unless otherwise specified.) The images are used to characterise the patterns in terms of the dot size and contrast between the dots and the background (Fig. 1 d,e). The regularity of the pattern was exploited to treat the data in reciprocal space to accurately locate the motifs and to enable measurement in case of sub-optical resolution 250 nm size (see SI Fig. 6). The size is reported as the full width at half maximum (FWHM) of the intensity profile of the dots, which in vast majority of the cases has a roughly Gaussian intensity profile but may sometimes be deformed, either showing an asymmetry or a depression in intensity at the center. The measured values agree reasonably well with the putative size.

We used the patterns to explore the open question of whether or not the clustering of T cell receptors, whose engagement leads to actin polymerization and cell spreading, explicitly influences the actin architecture in T cells. T cells from the Jurkat cell line were allowed to interact with patterns bearing anti-CD3 for thirty minutes after which they were fixed and the F-actin (or TCR) was marked using fluorescent phalloidin (or antibody) following standard procedures (see SI for details). This duration of spreading ensures that the cells are fully spread but have not yet started retracting. The substrates, bearing the fixed cells, were imaged in the NaV channel to visualize the dots, and in the actin (or TCR) channel to visualise the cytoskeleton (or TCR). In addition, they were also imaged in reflection interference contrast microscopy (RICM) that clearly demarcates the extent of cell spreading and reveals membrane topography.[42]

As can be seen in Fig. 2 a, the cells spread on the patterned surface, forming contacts of variable intimacy (as seen from grey scales in RICM). Unlike in some of our previous work with cells on similar patterns formed by self-assembled colloidal beads, no correlation between membrane topography, as revealed by RICM grey scale, is immediately discernible.[36,43] The spread-area of the whole cell was quantified as described before.[36,43] Interestingly, the pattern-type does not influence the area. Rather, it is correlated with the average surface density of the protein (as inferred from the fluorescence intensity) as expected from previous work[36](Fig. 2 b). Gathering data from those samples that have similar surface density,

no statistical difference between cell area on different pattern-types was found (Fig. 2 c). The global actin organization was homogenous (Fig. 2 d) as quantified by a peripherality parameter p defined as ratio of average intensity of the whole cell and that at the center. Theoretically, this parameter is expected to be $\gg 1$ if the actin is peripherally distributed (as is the case on homogeneously coated substrate[42] and ≤ 1 if it is homogeneous. Here, actin is seen to be mostly homogeneous on patterned substrates with $0.6<p<1.5$ for majority of cells (see SI for definition of p), however, few cells also show peripheral organization.

At the cluster-scale, TCR is seen to be clustered according to the underlying NaV pattern[36,43] (see SI Fig. 7), but visual inspection and conventional image analysis do not show any hint of the presence of the underlying dots on the local topography of membrane imaged in RICM or the local architecture of the actin cytosckeleton imaged in TIRF (Fig. 2 a). The repeated identical clusters however provide an opportunity to delve further into the question to ascertain whether or not ligand clustering has an effect on local cell architecture. The repeated motifs provide a template to extract, from the image of a whole cell, the structure of actin or membrane on top of a ligand cluster (on) or next to a ligand cluster (off). A classifier is then trained to distinguish 'on' from 'off', and its ability to successfully do so for unseen data with better than random accuracy is taken as a marker for real difference between 'on' and 'off' architecture.

Briefly (see SI for details, SI Fig. 8-11, code available at https://github.com/ahmed344/AI-based-detection-of-T-cell-features), first the spatial coordinates of the lattice are identified and a square-shaped zone is designated around each lattice point. These zones are 'on-dot'. Next the lattice is shifted such that the new lattice-points are at the centroid of the triangles forming the original lattice, and similar 'off-dot' zones are created. For each cell, there are three image-channels: the NaV-channel imaging the underlying ligand array, the cell imaged in TIRF actin-channel and the cell imaged in RICM channel. For each channel, on or off dot mini-images are cut according to the on and off zones defined before (Fig. 3 a-d).

The on and off dot mini-images of actin (or the RICM mini-images) are fed to an image

classifier convolutional neural network (CNN) with 3 convolution layers. For each cell, the mini-images are randomly divided into two sets - a training-set with about 80% of the data and a validation-set with the rest. The model is trained for 5000 epochs. At each epoch, the model can only see the labels of the training data-set in order to fit its parameters to correct its classification (quantified as the loss factor) for the next epoch. The labels of the validation data-set remains unseen during fitting, but are used to calculate the loss and accuracy corresponding to the validation data-set. At the end of one training cycle (5000 epochs), the accuracy (defined as the proportion of correct identification) of the trained model corresponding to minimum loss is reported. Due to the small number of mini-images, the details of how the data is split into the training and validation data-sets affects the ability to fit a classifier network to the data. To account for this limitation, for each cell the training is repeated 100 times, each for a different partition of training and validation data-sets (see Fig. 3 e for a summary). As always, an accuracy of 1 corresponds to all the mini-images being classified correctly, and a value of 0.5 is expected if the classification is totally random. It is noticed that for the majority of cells, the accuracy is largely skewed towards values greater than 0.5 for most choice of the sets, and reaches the value of 1 for at least one choice of sets (Fig. 3 f).

To eliminate the possibility of bias, we compare these experiments with a negative control, consisting of exactly the same experiment except that the cells now adhere to a homogeneously coated surface. A "fake" lattice is imposed on the images and mini-images on and off dots are prepared, and exactly the same algorithm is applied. Here, the accuracy is less skewed towards larger values and only two cells reach an accuracy of 1 for at least one choice of sets (Fig. 3 g).

Comparing the histograms of accuracy for the E700 substrates (Fig. 3 h), it is confirmed that the accuracy distributions on the two kinds of substrates are very different. On homogeneous substrates, the accuracy distribution peaks close to 0.5 (median = 0.57, median absolute deviation (MAD) = 0.05), as expected for random classification. However,

the distribution on the patterns is skewed further towards 1 (median = 0.64, MAD = 0.1), corresponding to correct classification of 'on' or 'off' dot. We therefore conclude that on a homogeneous substrate, there is no discernible difference in actin organization between 'on' or 'off' dot as expected since the designation 'on' or 'off' is perfectly arbitrary. However, on a pattern, there is indeed a difference between organization 'on' and 'off' dot. Stronger conclusions can be drawn for the RICM data based both on individual cells (SI Fig. 13) and histograms (Fig. 3 i, homogeneous: median = 0.58, MAD = 0.08; pattern: median = 0.75, MAD = 0.12). For both actin and RICM data, a statistical comparison of the distribution of the accuracy in the pattern and homogeneous case using Mann-Withney-Wilcoxon rank test for unpaired data confirms the conclusion that the populations are indeed different ($p < 0.0001$). Similar conclusions can be drawn for the E400 substrates (SI Fig. 14, 15).

It is important to note that our approach differs from the classical classification problem where two categories of objects to be classified are a priori known to be different. In that case, after training, the CNN is usually required to classify any number of unseen data, enabling automation of repetitive or specialized tasks. Here, we are using the classifier to test whether the two categories of objects are sufficiently different. The CNN is first shown images that come from two different origins, and thus form two different categories, even though it is not known if they are actually different in terms of appearance. The CNN is then required to categorise randomly selected images - correct classification, with the success rate significantly better than random assignment, means that the images are indeed different in appearance, even though the nature of this "hidden feature" is not revealed by this approach.

This 'blind' deep-learning approach is not dependent on any specific model or any assumption about the architecture of the T cell. A priory, TCR distribution could be expected to impact actin architecture even though no such effect was so far reported at the sub-micron scale. The method introduced here unambiguously shows that clustering of TCR does indeed locally modify the cytoskeleton, a conclusion that could not be conclusively drawn based on conventional image analysis (SI Fig. 16-18). *A posteriori* analysis hints that some cells

may show actin depletion on top of ligand/receptor clusters (SI Fig. 18) but further experiments with super-resolution microscopy or even electron microscopy on roofed-cells may be necessary to reveal the detailed structure and mechanism of the modification. Our coupled patterned stimulation / AI based analysis workflow will be fully applicable to superresolution images.

The nano-fabrication and the analysis technique presented here can each be used independently of the other. The nano-fabricated surfaces are very versatile in terms of geometry(see SI Fig. 19) as well as chemistry. Being composed only of organic molecules with minimal interaction with light, they can be used with any optical technique, even if the clusters are dense, quite challenging with more commonly used gold nano-dots due to possibility of creating surface excitations. The presence of identical repeated clusters of stimulation, here anti-CD3 μ-clusters, generates large number of presumably identical response – which, when contrasted with response off the stimulation-zone, can be catagorised in a binary fashion. The binary data can then be fed to an AI classifier, which classifies the data into on-cluster or off-cluster response. The new idea here was to use the ability of the classifier to correctly classify, as a marker of difference. This 'blind' strategy can be generalised to any situation where a subtle response is expected but its nature is not known *a priori*. Once the presence of a response is ascertained, it may then be easier to detect it. Beyond specific uses similar to one here, this recipe can be used in design of high-throughput diagnosis where on one hand sub-cellular and repeated stimulations increase the number of readouts per cell, and on the other hand a 'blind' deep-learning strategy, dependent on presence of large amount of input data, simplifies analysis and interpretation.

Acknowledgement

We thank Etienne Loiseau for careful reading of the manuscript. Electron beam lithography, metallization and electron microscopy were performed in PLANETE CT PACA clean room facility. We thank M. Biarnes-Pelicot (LAI) and L. Borges (PCC) for help with cells. This work was partially funded by the European Research Council via grant No. 307104 FP/2007-2013/ERC, ANR via grant 18-CE92-0033-microCJ, Partial funding was also provided by SATT Sud-Est and Turing Centre for Living Systems.

Supporting Information Available

Details of experimental methods, imaging, data analysis, image analysis using deep learning algorithm and conventional image analysis, schematic of the fabrication process and functionalisation, SEM images at different fabrication steps, fluorescent image of TCR colocalisation, complete accuracy data for all studied samples and conditions, proof-of-principle demonstration of asymmetric motifs. The Supporting Information is available free of charge on the ACS Publications website

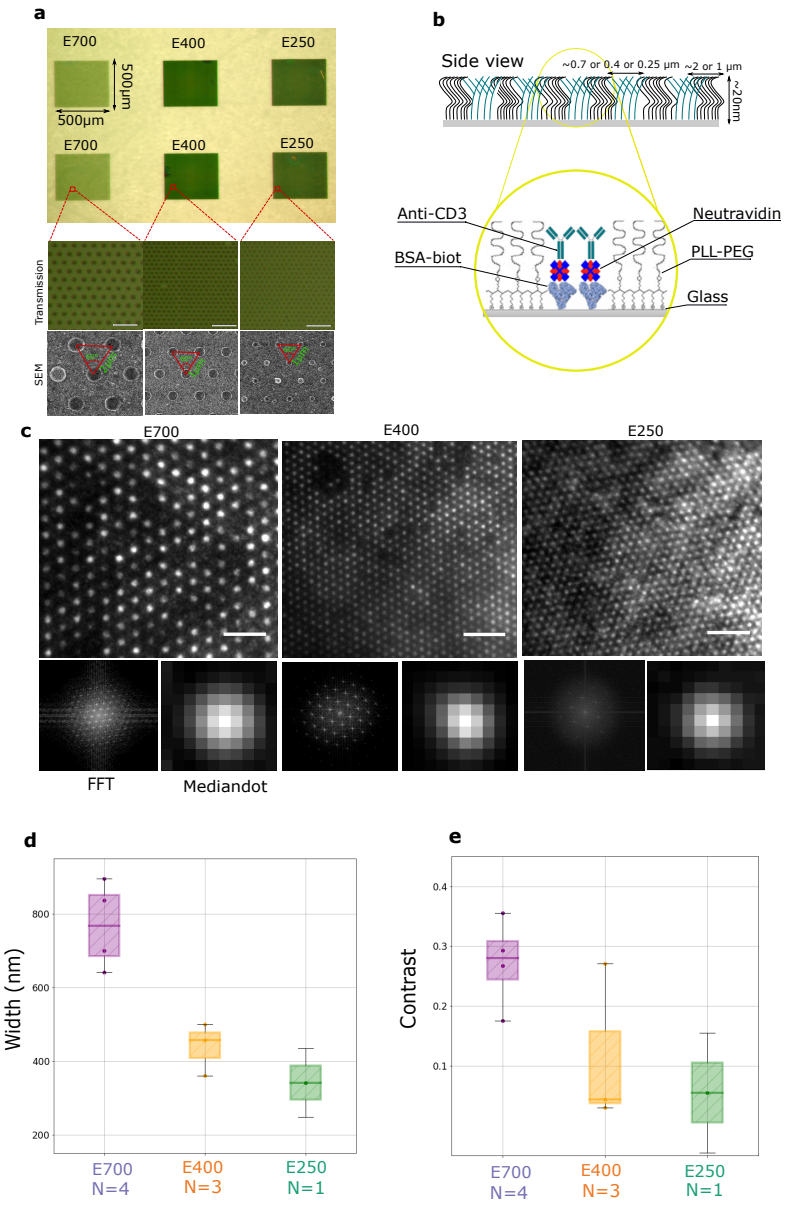

Figure 1: **Pattern characterisation**. **a**. Top: Overview of a patterned cover slip. Each square may present a different motif (the difference in color arises due to the difference in the size and spacing of the dots; the smaller the dots, the darker the color). From left to right - name (putative diameter - pitch): E700 (700 nm-2μm), E400 (400 nm-1μm), E250 (250 nm-1μm). Bottom: bright field (transmission) / scanning electron microscopy (SEM) image. **b**. Schematic of the patterned substrates (not to scale, side view and its zoom). **c**. Examples of epi-fluorescence images for (left to right) E700, E400 and E250 with corresponding fast Fourier transform (FFT) and a 'median' dot of each field; **d,e**. Quantification of the size (FWHM) (**d**), and contrast (**e**) of the antibody nano-dots from fluorescence images of the underlying Neutravidin pattern. Scale bar=5 μm.

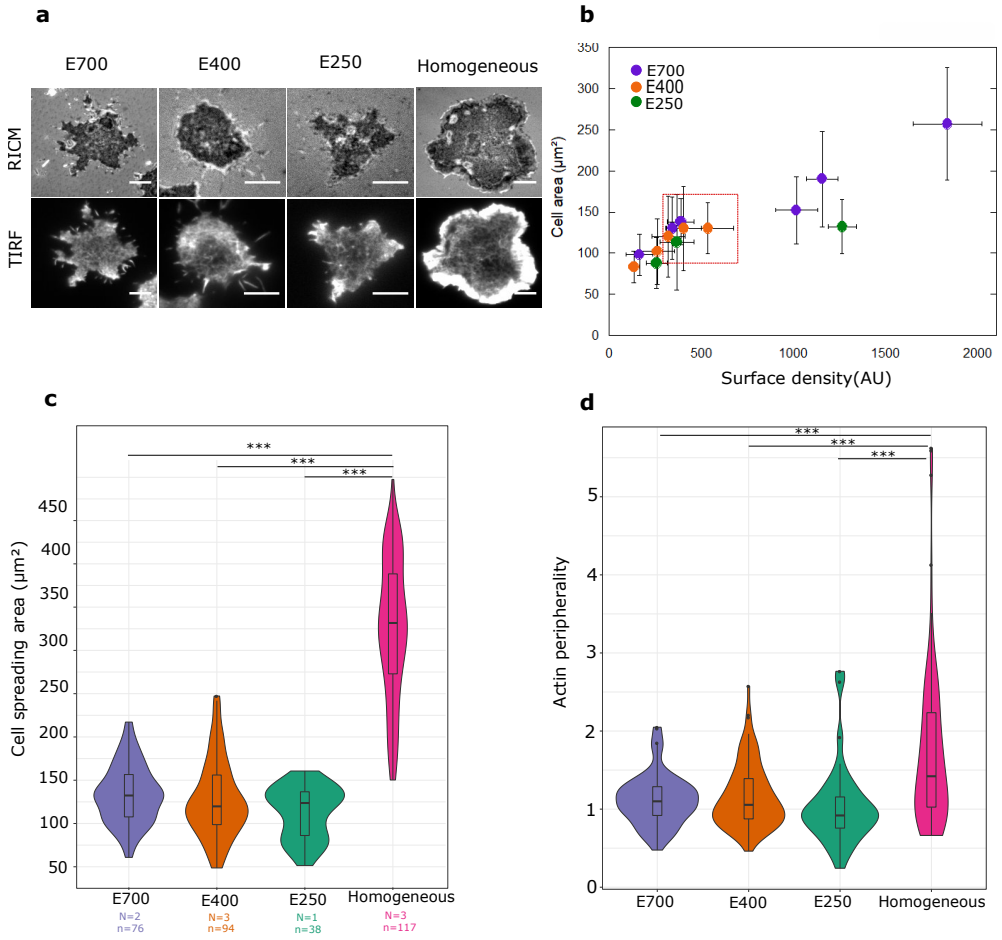

Figure 2: **Impact of anti-CD3 clustering on cell adhesion and actin organisation**. **a**. RICM images (top) and TIRF images (bottom) of the actin labeled cells on E700, E400, E250 patterns or homogeneously functionalised control. **b**.Plot of cell area as a function of average ligand surface density for the three different types of pattern. Each point represents one experiment with around 40 cells. Data in the red box are used in c. **c**.Violin plot of cell spreading area measured from RICM images for the patterned substrates with comparable surface density (red-box in b). **d**. Violin plot of actin peripherality calculated from TIRF images for cases shown in b and on homogeneous control substrate. Scale bar=10 μm.

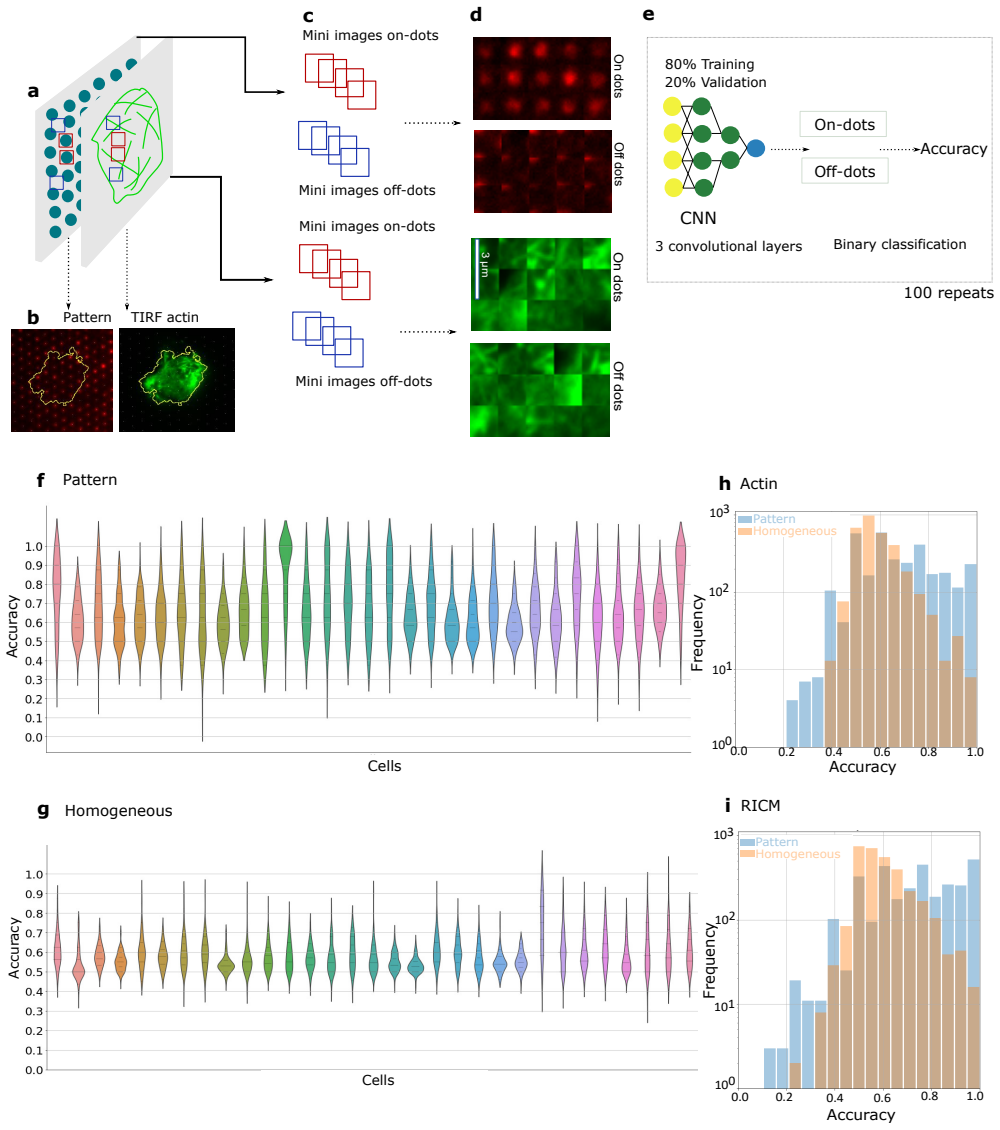

Figure 3: **a**. Schematic for generation of the mini-images of actin. Red (blue) squares correspond to on- (off-) dot zones. **b**. Epi-fluorescent image of the pattern and TIRF image of actin of a cell on the pattern. **c,d**. Schematic and real example of mini-images on- or off-dot. **e**. Schematic of the working of the image classifier. **f,g**. Violin plot of cell-by-cell accuracy for 100 different repeats on pattern and homogeneous substrates in actin channel. **h,i**. Histograms of accuracy pooling all repeats for all cells, comparing pattern and homogeneous substrates for actin (h) and RICM (i).

References

(1) Whitesides, G.; Ostuni, E.; Takayama, S.; Jiang, X.; Ingber, D. E. Soft lithography in biology and biochemistry,. *Annual review of biomedical engineering* **2001**, *3*, 335–373.

(2) Filipponi, L.; Livingston, P.; Kaspar, O.; Tokarova, V.; Nicolau, D. V. Protein patterning by microcontact printing using pyramidal pdms stamps. *Biomed Microdevices.* **2016**, *18*, 1–7.

(3) Spatz, J.; Geiger, B. Molecular engineering of cellular environments: cell adhesion to nano-digital surfaces. *Methods in cell biology* **2007**, *83*, 89–111.

(4) Schvartzman, M.; Palma, M.; Sable, J.; Abramson, J.; Hu, X.; Sheetz, M.; Wind, S. Nanolithographic control of the spatial organization of cellular adhesion receptors at the single-molecule level. *Nano letters* **2011**, *11*, 1306–1312.

(5) Platzman, I.; Gadomska, K. M.; Janiesch, J.-W.; I. Louban, E. A. C.-A.; P.Spatz, J. Soft/elastic nanopatterned biointerfaces in the service of cell biology. *Methods in cell biology* **2013**, *119*, 237–260.

(6) Biswas, A.; Bayer, I. S.; Biris, A. S.; Wang, T.; Dervishi, E.; Faupel, F. Advances in top-down and bottom-up surface nanofabrication: Techniques, applications and future prospects. *Adv Colloid Interface Sci.* **2012**, *170*, 2–27.

(7) Moon, J. J.; Huang, B.; Irvine, D. J. Engineering nano-and microparticles to tune immunity. *Advanced mat* **2012**, *24*, 3724–3746.

(8) Pi, F.; Dillard, P.; Limozin, L.; Charrier, A.; Sengupta, K. Nanometric protein-patch arrays on glass and polydimethylsiloxane for cell adhesion studies. *Nano Letters* **2013**, *13*, 3372–3378.

(9) Pi, F.; Dillard, P.; Alameddine, R.; Benard, E.; Wahl, A.; Ozerov, I.; Charrier, A.;

Limozin, L.; Sengupta, K. Size-Tunable Organic Nanodot Arrays: A Versatile Platform for Manipulating and Imaging Cells. *Nano letters* **2015**, *15*, 5178–5184.

(10) Hawkes, W.; Huang, D.; Reynolds, P.; Hammond, L.; Ward, M.; Gadegaard, N.; Marshall, J.; Iskratsch, T.; Palma, M. Probing the nanoscale organisation and multivalency of cell surface receptors: DNA origami nanoarrays for cellular studies with single-molecule control. *Faraday Discussions* **2019**, *219*, 203–219.

(11) Penzo, E.; Wang, R.; Palma, M.; Wind, S. Selective placement of DNA origami on substrates patterned by nanoimprint lithography. *Journal of Vacuum Science & Technology B* **2011**, *29*, 06F205.

(12) Tikhomirov, G.; Petersen, P.; Qian, L. Fractal assembly of micrometre-scale DNA origami arrays with arbitrary patterns. *Nature* **2017**, *552*, 67–71.

(13) Shen, W.; Zhong, H.; Neff, D.; Norton, M. NTA directed protein nanopatterning on DNA Origami nanoconstructs. *Journal of the American Chemical Society* **2009**, *131*, 6660–6661.

(14) Falconnet, D.; Koenig, A.; Assi, F.; Textor, M. A combined photolithographic and molecular-assembly approach to produce functional micropatterns for applications in the biosciences. *Advanced Functional Materials* **2004**, *14*, 749–756.

(15) Gopinath, A.; Rothemund, P. W. Optimized assembly and covalent coupling of single-molecule DNA origami nanoarrays. *Acs Nano* **2014**, *8*, 12030–12040.

(16) Weigert, M.; Schmidt, U.; Boothe, T.; Müller, A.; Dibrov, A.; Jain, A.; Wilhelm, B.; Schmidt, D.; Broaddus, C.; Culley, S., et al. Content-aware image restoration: pushing the limits of fluorescence microscopy. *Nature Methods* **2018**, *15*, 1090–1097.

(17) Belthangady, C.; Royer, L. Applications, promises, and pitfalls of deep learning for fluorescence image reconstruction. *Nature Methods* **2019**, *16*, 1215–1225.

(18) Moen, E.; Bannon, D.; Kudo, T.; Graf, W.; Covert, M.; Van Valen, D. Deep learning for cellular image analysis. *Nature Methods* **2019**, *16*, 1233–1246.

(19) Wang, H.; Rivenson, Y.; Jin, Y.; Wei, Z.; Gao, H., R.and Günaydın; Bentolila, L.; Kural, C.; Ozcan, A. Deep learning enables cross-modality super-resolution in fluorescence microscopy. *Nature methods* **2019**, *16*, 103–110.

(20) Killops, K. L.; Gupta, N.; Dimitriou, M. D.; Lynd, N. A.; Jung, H.; Tran, H.; Bang, J.; Campos, L. M. Nanopatterning biomolecules by block copolymer self-assembly. *ACS Macro Letters* **2012**, *1*, 758–763.

(21) Kaizuka, Y.; Douglass, A. D.; Varma, R.; Dustin, M. L.; Vale, R. D. Mechanisms for segregating T cell receptor and adhesion molecules during immunological synapse formation in Jurkat T cells. *Proc. Natl. Acad. Sci. U.S.A* **2007**, *104*, 2029620–301.

(22) Yokosuka, T.; Sakata-Sogawa, K.; Kobayashi, W.; Hiroshima, M.; Hashimoto-Tane, A.; Tokunaga, M.; Dustin, M. L.; Saito, T. Newly generated T cell receptor microclusters initiate and sustain T cell activation by recruitment of Zap70 and SLP-76. *Nat. Immunol.* **2005**, *6*, 1253–1262.

(23) Varma, R.; Campi, G.; Yokosuka, T.; Saito, T.; Dustin, M. L. T Cell Receptor-Proximal Signals Are Sustained in Peripheral Microclusters and Terminated in the Central Supramolecular Activation Cluster. *Immunity* **2006**, *25*, 117–127.

(24) Bunnell, S. C.; Hong, D. I.; Kardon, J. R.; Yamazaki, T.; McGlade, C. J.; Barr, V. A.; Samelson, L. E. T cell receptor ligation induces the formation of dynamically regulated signaling assemblies. *J. Cell. Biol.* **2002**, *158*, 1263–1275.

(25) Hong, J.; Murugesan, S.; Betzig, E.; Hammer, J. A. Contractile actomyosin arcs promote the activation of primary mouse T cells in a ligand-dependent manner. *PLoS One* **2017**, *12*, 1–22.

(26) Yi, J.; Wu, X. S.; Crites, T.; Hammer, J. A. Actin retrograde flow and actomyosin II arc contraction drive receptor cluster dynamics at the immunological synapse in Jurkat T cells. *Mol. Biol. Cell* **2012**, *25*, 834–852.

(27) Murugesan, S.; Hong, J.; Yi, J.; Li, D.; Beach, J. R.; Shao, L.; Meinhardt, J.; Madison, G.; Wu, X.; Betzig, E.; Hammer, J. A. Formin-generated actomyosin arcs propel T cell receptor microcluster movement at the immune synapse. *J. Cell Biol.* **2016**, *3*, 383–399.

(28) Doh, J.; Irvine, D. J. Immunological synapse arrays: patterned protein surfaces that modulate immunological synapse structure formation in T cells. *Proceedings of the National Academy of Sciences* **2006**, *103*, 5700–5705.

(29) Shen, K.; Thomas, V. K.; Dustin, M. L.; Kam, L. C. Micropatterning of costimulatory ligands enhances CD4+ T cell function. *Proc Natl Acad Sci U S A* **2008**, *105*, 7791–7796.

(30) Mossman, K. D.; Campi, G.; Groves, J. T.; Dustin, M. L. Altered TCR Signaling from Geometrically Repatterned Immunological Synapses. *Science* **2005**, *310*, 1191–1193.

(31) Manz, B. N.; Jackson, B. L.; Petit, R. S.; Dustin, M. L.; Groves, J. T. T-cell triggering thresholds are modulated by the number of antigen within individual T-cell receptor clusters. *Proceedings of the National Academy of Sciences* **2011**, *108*, 9089–9094.

(32) Smoligovets, A. A.; Smith, A. W.; Wu, H.-J.; Petit, R. S.; Groves, J. T. Characterization of dynamic actin associations with T-cell receptor microclusters in primary T cells. *Journal of cell science* **2012**, *125*, 735–742.

(33) Bashour, K. T.; Gondarenko, A.; Chen, H.; Shen, K.; Liu, X.; Huse, M.; Hone, J. C.; Kam, L. C. CD28 and CD3 have complementary roles in T-cell traction forces. *Proc Natl Acad Sci U S A* **2014**, *111*, 2241–2246.

(34) Liu, Y.; Blanchfield, L.; Ma, V. P.-Y.; Andargachew, R.; Galior, K.; Liu, Z.; Evavold, B.; Salaita, K. DNA-based nanoparticle tension sensors reveal that T-cell receptors transmit defined pN forces to their antigens for enhanced fidelity. *Proceedings of the National Academy of Sciences* **2016**, *113*, 5610–5615.

(35) Tabdanov, E.; Gondarenko, S.; Kumari, S.; Liapis, A.; Dustin, M.; Sheetz, M.; Kam, L. C.; Iskratsch, T. Micropatterning of TCR and LFA-1 ligands reveals complementary effects on cytoskeleton mechanics in T cells. *Integrative Biology* **2015**, *7*, 1272–1284.

(36) Dillard, P.; Pi, F.; Lellouch, A.; Limozin, L.; Sengupta, K. Nano-clustering of ligands on surrogate antigen presenting cells modulates T cell membrane adhesion and organization. *Integrative Biology* **2016**, *8*, 287–301.

(37) Cai, H.; Muller, J.; Depoil, D.; Mayya, V.; Sheetz, M. P.; Dustin, M. L.; Wind, S. J. Full control of ligand positioning reveals spatial thresholds for T cell receptor triggering. *Nature nanotechnology* **2018**, *13*, 610–617.

(38) Delcassian, D.; Depoil, D.; Rudnicka, D.; Liu, M.; Davis, D. M.; Dustin, M. L.; Dunlop, I. E. Nanoscale ligand spacing influences receptor triggering in T cells and NK cells. *Nano letters* **2013**, *13*, 5608–5614.

(39) Deeg, J.; Axmann, M.; Matic, J.; Liapis, A.; Depoil, D.; Afrose, J.; Curado, S.; Dustin, M. L.; Spatz, J. P. T cell activation is determined by the number of presented antigens. *Nano letters* **2013**, *13*, 5619–5626.

(40) Matic, J.; Deeg, J.; Scheffold, A.; Goldstein, I.; Spatz, J. P. Fine tuning and efficient T cell activation with stimulatory aCD3 nanoarrays. *Nano letters* **2013**, *13*, 5090–5097.

(41) Benard, E.; Pi, F.; Ozerov, I.; Charrier, A.; Sengupta, K. Ligand nano-cluster arrays in a supported lipid bilayer. *JoVE (Journal of Visualized Experiments)* **2017**, *122*, e55060.

(42) Dillard, P.; Varma, R.; Sengupta, K.; Limozin, L. Ligand-mediated friction determines morphodynamics of spreading T cells. *Biophysical Journal* **2014**, *107*, 2629–2638.

(43) Benard, E.; Nunès, J. A.; Limozin, L.; Sengupta, K. T cells on engineered substrates: The impact of TCR clustering is enhanced by LFA-1 engagement. *Frontiers in immunology* **2018**, *9*, 2085.